Detection of Marine Vessel Transits in Spectrograms by Support Vector Machine

Kristian Darlington
Department of Software Engineering
University of Victoria
Victoria, Canada
kristiandarlington.com

***Abstract*—Tracking and analyzing trends in marine vessel traffic is paramount in maintaining the wellbeing of marine species living amongst human activity. Currently, volunteer scientists at the Saturna Island Marine Research and Education Society (SIMRES) must analyze acoustic data – presented in the form of spectrograms – recorded from their underwater hydrophones manually. This paper details a system that can automate the detection of marine vessel transits through the use of simple spectrogram preprocessing, feature extraction, and classification by support vector machine.**

***Keywords*—spectrogram, classification, SVM, marine.**

I. Overview

The Saturna Island Marine Research and Education Society (SIMRES), a registered non-profit organization based on Saturna Island in British Columbia, Canada, has set up a number of underwater hydrophones off the coast of British Columbia that record acoustic data throughout each day [1]. The acoustic data from each hydrophone is stored in five-minute intervals, which can then be viewed as a spectrogram and visually analyzed for the presence of marine vessels transiting near the hydrophone.

Currently, SIMRES technicians must manually analyze each spectrogram and flag those that contain marine vessel transits. This process provides insight into human activity that can be cross-correlated with the observed behaviours of marine species in the surrounding area, thus allowing SIMRES and other like-organizations to make educated decisions regarding improvements to the state of marine ecosystems.

The manual review of spectrogram data is time consuming for technicians whose efforts would be more valuable elsewhere: a lack of automation that this project hopes to address. A solution that can automatically and reliably classify spectrograms as containing vessel transits or not containing vessel transits would save hours of labour.

II. Literary Review

In researching possible existing solutions to the problem of detecting marine vessel transits in spectrograms, there were no papers found that address the exact issue at hand. This is not to say that none exist, but only that none were found. A number of papers addressing similar problems were reviewed, however. Two papers that inspired elements of the approach used in this project are "Detection and Classification of Right Whale Calls Using an 'Edge' Detector Operating on a Smoothed Spectrogram" by Douglas Gillespie and "A Deep Learning-based Framework for the Detection of Schools of Herring in Echograms" by Alireza Rezvanifar et al. [2], [3].

In Gillespie's paper, the problem addressed is the automated detection of right whale calls in spectrograms generated by undersea acoustic hydrophones off the east coast of Canada and the United States. In a spectrogram, a right whale call appears as an upswept curve, distinguishing itself from most, but not all, marine noises [2]. Other whales exist that make similar calls and these, along with marine vessel noise and other environmental noise, must be filtered out during the detection process. Figure 1, taken from Gillespie's paper, shows a right whale call in a spectrogram.

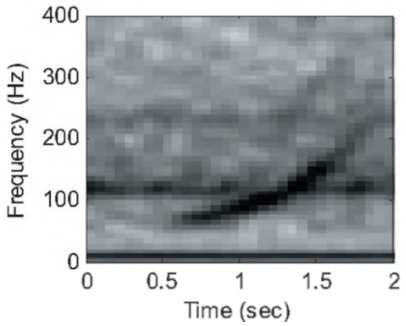

Figure 1: Spectrogram showing a right whale call [2].

The proposed approach in Gillespie's paper consists of smoothing a spectrogram to reduce impulse noise, detecting the "edges" of sounds, computing attributes of each sound regarding duration and frequency, then running those attributes through a multivariate discriminant analysis function for final classification.

Rezvanifar et al.'s project attempts to automate the detection of schools of herring in spectrograms, which generally appear as brief and high amplitude, vertically elongated shapes when compared with other background noise [3]. Figure 2, taken from Rezvanifar et al.'s paper, shows a school of herring in a spectrogram.

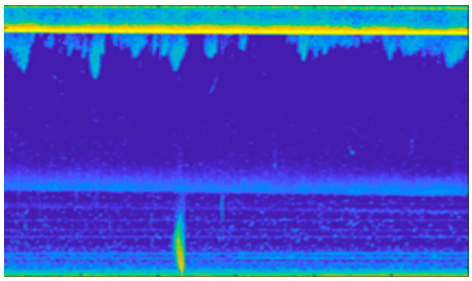

Figure 2: Spectrogram showing a vertically elongated shape characteristic of a school of herring (bottom center) [3].

The approach taken by Rezvanifar et al. to automate the detection of schools of herring consists of smoothing the image along the time axis, binarizing the image with adaptive thresholding, filling in gaps and removing protrusions via morphological opening and closing, and taking steps to filter out connected components unlikely to be a school of herring. The bounding boxes corresponding to the remaining regions of interest are then processed by a convolutional neural network [3].

With the problem domains of Gillespie's project and Rezvanifar et al.'s project consisting of the detection of right whale call upsweeps and short impulses generated by schools of herring, respectively, neither paper can be said to solve the exact problem of detecting vessel transits. In fact, there exists room for improvement in each paper's problem domain based on the results provided [2], [3].

The remainder of this paper details the approach taken to automatically detect vessel transits in spectrograms (Section III), results of this approach and methods used to evaluate these results (Section IV), and an overall conclusion providing a brief summary and plans for future work (Section V). References are listed in Section VI.

III. Proposed Approach

This section is broken up into two parts. Section III. A. details the approach taken by Gillespie to solve the problem domain of his paper detailed in Section II, while Section III. B. details the approach taken to solve this project's problem domain.

A. Detection of Right Whale Calls in Spectrograms

The primary source paper that this project's approach is based on is "Detection and Classification of Right Whale Calls Using an 'Edge' Detector Operating on a Smoothed Spectrogram" by Douglas Gillespie, in which a two-stage process is used to detect right whale call upsweeps in spectrograms [2]. The first stage smooths the spectrogram via convolution with a Gaussian kernel to remove impulse noise, then detects the edges of "sounds" using a threshold edge detector that adaptively compares the amplitude of each pixel with the background amplitude at the same frequency. The second stage involves feature extraction and classification, which is carried out by determining statistics of each detected "sound," then entering those variables into a multivariate discriminant analysis function.

The Gaussian kernel, *K*, convolved with the spectrogram in Gillespie's paper is three-by-three of the form

$$K = \begin{matrix} 1 & 2 & 1 \\ 2 & 4 & 2 \\ 1 & 2 & 1 \end{matrix}.$$

The edge detection algorithm compares the amplitude of each pixel in a row, $S'_{(t,f)}$, with a continuously updating background measurement, $B_{(t,f)}$. The background value is updating with the formula

$$B_{(t,f)} = B_{(t-1,f)} + \frac{S'_{(t,f)} - B_{(t-1,f)}}{\alpha}$$

where α is a time constant that is set based on an heuristic detailed below. Spectrogram regions over threshold were marked as an edge, determined by the equation

$$\frac{S'_{(t,f)}}{B_{(t,f)}} > Thresh$$

where, for the purposes of right whale calls, $Thresh$ was set to 6 dB.

If a pixel was above threshold, α would be set to 160 (providing a time interval of approximately ten seconds), while α would be set to 16 (providing a time interval of approximately one second) if the pixel was below threshold. The reason for this changing time constant was to account for an increasing trend in $B_{(t,f)}$ when the surrounding sound was above the average noise of the image [2].

Marked edges at different frequencies were then connected vertically with other edges detected in the same time slice, closing off open gaps in a shape and hopefully forming one complete "sound." A buffer of one below-threshold time slice was allowed between edges to prevent sounds that rose above and fell below threshold from being excluded.

Extraction of features from the spectrograms is done in a simple manner by which, for each detected sound, metadata of the spectrogram (i.e. the bandwidth and time duration that a single pixel represents) is used to convert pixel counts to measurements in decibels and seconds. This is likely done by searching the spectrogram for a sound and following the outer edge encompassing the sound, but it is not detailed in the paper. The desired features were duration, start frequency, minimum frequency, sweep frequency, maximum instantaneous bandwidth, and positions of the minimum and maximum frequency.

Sounds were initially separated into right whale calls and non-right whale calls by filtering them on minimum duration, maximum duration, start frequency, and sweep frequency. After this, sounds that had not been filtered out were entered into a multivariate discriminant analysis function that took start frequency, sweep frequency, duration, and maximum instantaneous bandwidth as input and reduced dimensionality. A cut would be made on the first canonical variable output from the analysis, allowing for the final separation of sounds into right whale calls and non-right whale calls [2].

B. Detection of Vessel Transits in Spectrograms

While the spectrograms and use of undersea acoustic hydrophones are similar between this project and Gillespie's project detailed in Section III. A., the entities to be detected greatly differ. Due to marine vessels ranging in size from pleasure craft to container ships, the amplitude, tone bandwidths, duration, and overall patterns seen in spectrograms for vessel transits vary drastically. Ships can also be passing in the distance or nearby. They can pass behind an obstruction, like an island, and reappear. There is

no fixed shape to search for, but there are trends in the data that routinely appear when a vessel transit is present.

Two patterns existing in spectrograms that technicians at SIMRES use to reliably determine a vessel's presence are Lloyd's mirror pattern, appearing as a sequence of U-shapes entities, and long, high power tones at one or more frequencies. Lloyd's mirror pattern is often difficult to see if the vessel is not close to the hydrophone, but tones are almost always distinguishable if there is a transit.

With tonal patterns and Lloyd's mirror pattern being the primary elements used by human analysts to detect vessel transits, they seemed appropriate targets for the automated system. As such, the approach used in this project consists of four sections:

1) Preprocessing
2) Primary tone detection
3) Lloyd's mirror pattern detection
4) SVM classification

Sections III. B. 1), 2), 3), and 4) elaborate on these processes in detail.

1) Preprocessing

The early preprocessing step is based on the first stage of Gillespie's paper, in which a Gaussian kernel is convolved over the spectrogram and an adaptive thresholding algorithm binarizes it. Before this, however, the spectrogram is converted to a grayscale image from its colour representation because, while a colour image may help humans understand the power spectral density at a given point, grayscale is easier to manage for classification.

Up to 47 different colours are used in each spectrogram to indicate the approximate power spectral density at a given pixel. Each of these colours is converted to a shade of gray from a distribution of 47 approximately equally spaced values increasing from 0 to 255. The pixel colour indicating the lowest power spectral density interval is converted to 0, the pixel colour indicating the next power spectral density interval is converted to 5, and so on with the maximum power spectral density interval being converted to 255. A colour spectrogram is shown in Figure 3.

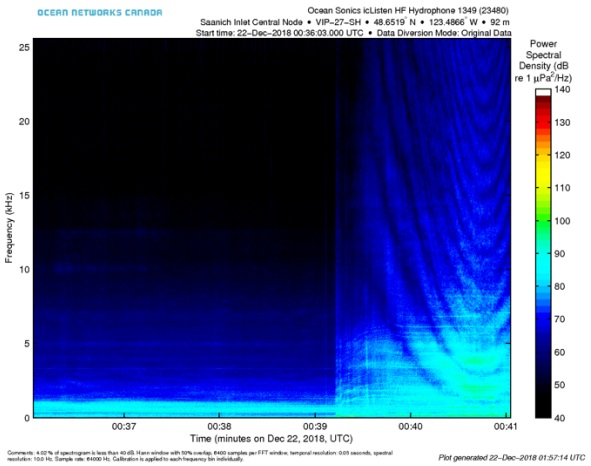

Figure 3: Spectrogram showing the tonal line patterns (left side) and Lloyd's mirror pattern (right side) that often mark a vessel transit.

The equivalent grayscale spectrogram to the colour spectrogram in Figure 3 is shown in Figure 4.

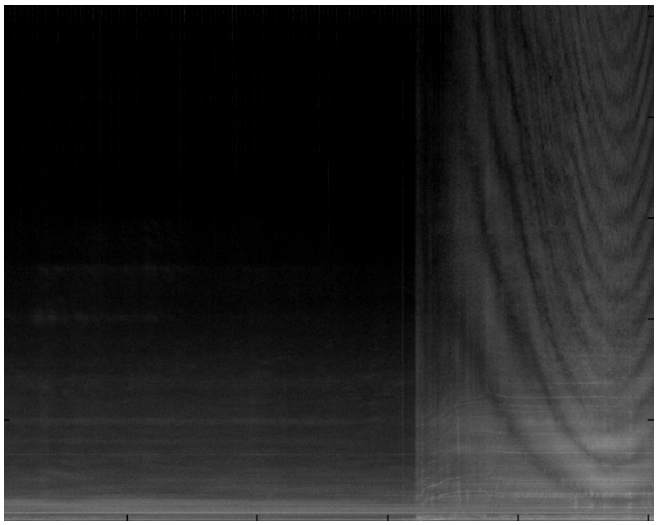

Figure 4: Same spectrogram as shown in Figure 3, converted to grayscale for easier processing.

The Gaussian kernel, K, used in this project was determined experimentally by reviewing the results of the smoothing algorithm on its own, as well as the results of the smoothing algorithm plus adaptive thresholding algorithm. Since vessel transits often produce large entities in the spectrograms, larger kernels were favoured over smaller kernels for the purpose of distributing intensity over larger areas. The kernel settled on was 7×7 with $\sigma_x = \sigma_y = 5$.

The adaptive thresholding algorithm used for this project was not the one detailed in Gillespie's paper, but instead the one used in Rezvanifar et al.'s paper and detailed in "Adaptive Thresholding using the Integral Image" by Derek Bradley and Gerhard Roth; a more generalized method of thresholding was desired that considered large bandwidths as opposed to a single frequency when determining the background noise level [3], [4]. This is due to the unpredictable variations in vessel noise. The method binarizes the spectrogram by computing the average value, a, of a rectangle of pixels around the pixel at (x, y) and, if

$$p(x, y) > a \times (100 - t)/100$$

where $p(x, y)$ is the pixel value at (x, y) and t is a threshold hyperparameter, the pixel at (x, y) is converted to white, or 255. If the above inequality does not hold true, the pixel at (x, y) is converted to black, or 0. The integral image, which significantly improves the performance of calculating the average pixel value of a rectangle, is computed using the equation

$$I(x, y) = f(x, y) + I(x - 1, y) + I(x, y - 1) - I(x - 1, y - 1)$$

where $I(x, y)$ is the value stored at each pixel and $f(x, y)$ is the sum of all pixel values to the left and above the point (x, y). The sum of any rectangle within the image can then be computed in constant time using the integral image by the equation

$$\sum_{x=x_1}^{x_2}\sum_{y=y_1}^{y_2} f(x,y) = I(x_2,y_2) - I(x_2,y_1-1) - I(x_1-1,y_2) + I(x_1-1,y_1-1)$$

Pseudocode for the algorithm, presented in Bradley and Roth's paper, is as follows:

```
procedure AdaptiveThreshold(in,out,w,h)
  for i = 0 to w do
    sum ← 0
    for j = 0 to h do
      sum ← sum + in[i,j]
      if i = 0 then
        intImg[i,j] ← sum
      else
        intImg[i,j] ← intImg[i-1,j] + sum
      end if
    end for
  end for
  for i = 0 to w do
    for j = 0 to h do
      x1 ← i - s/2 {border checking not shown}
      x2 ← i + s/2
      y1 ← j - s/2
      y2 ← j + s/2
      count ← (x2-x1)×(y2-y1)
      sum ← intImg[x2,y2] - intImg[x2,y1-1] -
            intImg[x1-1,y2] + intImg[x1-1,y1-1]
      if in[i,j]×count ≤ sum×(100-t)/100 then
        out[i,j] ← 0
      else
        out[i,j] ← 255
      end if
    end for
  end for
end procedure
```

where s is the ratio of the rectangle size for averaging versus the total dimensions of the input image (i.e. $s = 0.25$ would cause the rectangle dimensions to be one quarter of the width and one quarter of the height of the image) [4]. For this project, $t = -5$ and $s = 0.125$ was deemed appropriate through experimental analysis. A spectrogram binarized using this algorithm is shown in Figure 5, which is sourced from the grayscale spectrogram shown in Figure 4.

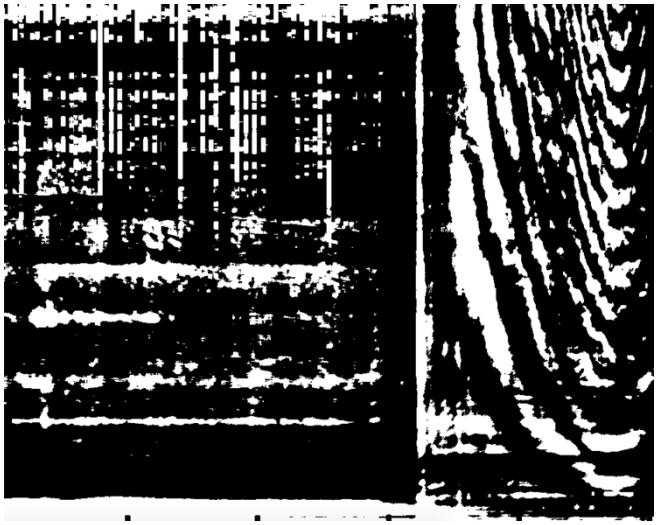

Figure 5: Spectrogram binarized with adaptive thresholding.

To find connected components, Grana's algorithm for eight-way pixel connectivity is used via the OpenCV open-source image processing library's *connectedComponentsWithStats* Python function [5]. The spectrogram in Figure 5 is shown in Figure 6 with connected components labelled by colour.

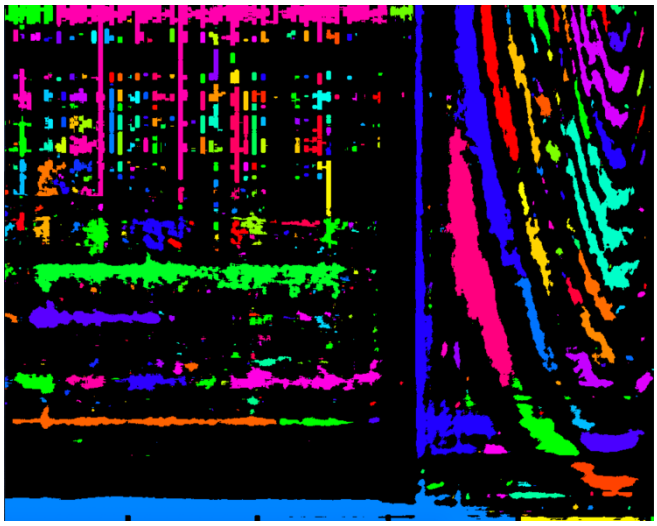

Figure 6: Connected components from Figure 5's spectrogram, now coloured.

Some connected components detail sounds of short duration, small bandwidths, or small area and are not meaningful to image classification. These are filtered out. For each connected component, those with < 80 pixels width (approx. 260 seconds), < 30 pixels height (approx. 1000 Hz), and/or < 300 pixels total size were filtered out. These values were determined experimentally by reviewing numerous preprocessed spectrograms and noting the general dimensions of connected components that appeared to be a consequence of a vessel transit. Figure 7 depicts the same spectrogram as Figure 6, but with connected components filtered out by the detailed criteria.

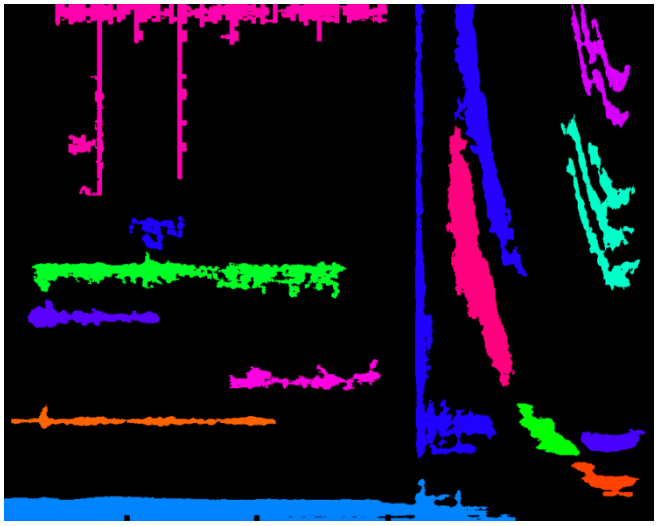

Figure 7: Connected components from Figure 6's spectrogram with short duration, small bandwidth, or few pixels are filtered out.

The binarized spectrogram with labelled and filtered connected components produced by these preprocessing steps is ready for feature extraction in Sections III. B. 2) and 3).

2) Primary Tone Detection

The primary tone detection step involves three processes in sequence: (1) generating a tone frequency duration histogram for each connected component in the input binarized spectrogram, (2) filtering tones in each connected component based on their durations, and (3) generating a tone frequency duration histogram of the longest-lasting tones over the entire spectrogram.

For each connected component, a duration versus frequency histogram with one bin per pixel in the frequency axis of the connected component is created. The number of pixels within a connected component at a particular pixel height (frequency) are summed to fill the respective bin for that height.

With a histogram of frequency durations for each connected component, the shortest 80% of tones are filtered out of each histogram, leaving the longest 20% of tones for each connected component. This percentile was chosen rather arbitrarily for the purpose of finding the longest-lasting, primary tones a vessel produced during its transit. The spectrogram depicted in Figure 7 is displayed in Figure 8 with the frequencies containing a longest-lasting tone of some connected component highlighted in red. These tones were found using the method described.

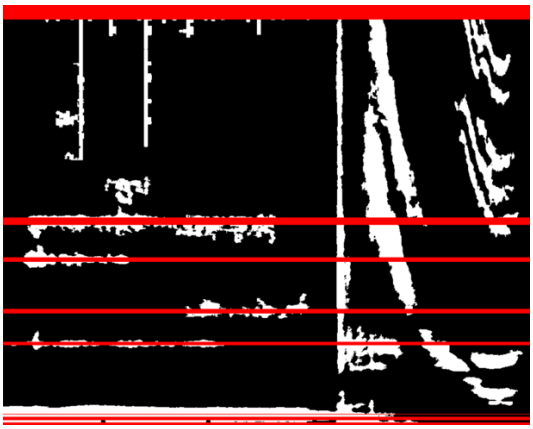

Figure 8: Binarized spectrogram with frequencies containing the longest-lasting tones of some connected component highlighted.

The same tonal frequencies are shown in Figure 9, overlaid on the original grayscale spectrogram in Figure 4.

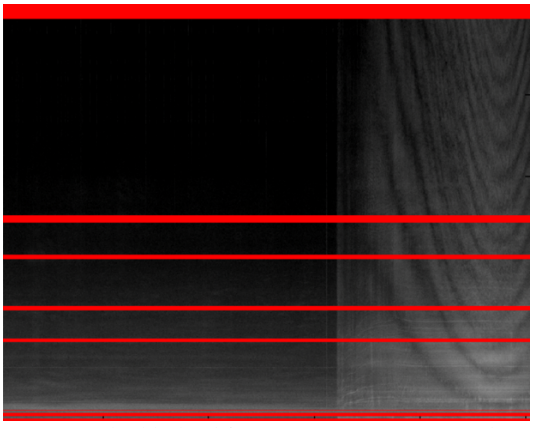

Figure 9: Same highlighted frequencies as in Figure 8, but on the original grayscale spectrogram.

A histogram of tone durations with thirteen bins, representing thirteen evenly spaced intervals of 57 pixels along the entire 741-pixel frequency axis of a spectrogram, is then generated. The durations of the longest-lasting tones computed in the previous step are summed by their height (frequency) in the spectrogram y-axis, f, to obtain d_f and binned into the two nearest bins according to the formulas

$$P_{f,2} = (f \bmod 57) \div 57$$
$$P_{f,1} = 1 - P_{f,2}$$

$$D_{f,2} = d_f \times P_{f,2}$$
$$D_{f,1} = d_f \times P_{f,1}$$

$$B_{f,1} = \lfloor f \div 57 \rfloor$$
$$B_{f,2} = (B_{f,1} + 1) \bmod 13$$

where $P_{f,1}$ and $P_{f,2}$ represent the percentage of tonal duration to enter the first bin and second bin, respectively; $D_{f,1}$ and $D_{f,2}$ represent the duration to enter the first bin and second bin, respectively; and $B_{f,1}$ and $B_{f,2}$ represent the first and second bin labels, respectively. This methodology is equivalent to a method of generating a histogram of gradients [6]. An issue that arises in this method is that a percentage of durations for tones above the highest frequency bin are added to the lowest frequency bin, which is not a problem when handling gradients angles due to $0° = 360°$. This problem could be solved by using a different method, but it was not deemed necessary due to the highest and lowest frequency bins often containing unremarkable information. The bulk of vessel transit information occurs in the midrange of the spectrogram.

The resulting 13×1 histogram is normalized by scaling its values to the range [0, 1] to improve SVM classification performance.

3) Lloyd's Mirror Pattern Detection

The method used to infer whether Lloyd's mirror pattern is present in a spectrogram is inspired by techniques used to detect hand gestures in other fields of image processing that use connected components, their convex hulls, and their convexity defects.

In analyzing the outputs of the connected components algorithm run on numerous spectrograms, it was observed that connected components associated with random marine noise and tonal patterns had few large convexity defects. Connected components associated with Lloyd's mirror pattern, however, often involved numerous large convexity defects due to their semblance to stacked parabolic curves with vertices. These curves would sometimes meld together during adaptive thresholding, which generated crevasses for defects. In testing, the points of maximum defect distance were often near the vertex of each "parabola." This fact is used to obtain a feature from the spectrograms: the number of large convexity defects.

For each connected component in a spectrogram, a convex hull was generated using the OpenCV open-source library's

convexHull Python function, which uses Sklansky's algorithm for computation [5]. A copy of Figure 7 is shown in Figure 10, but with convex hulls overlaid in blue and with colourless connected components.

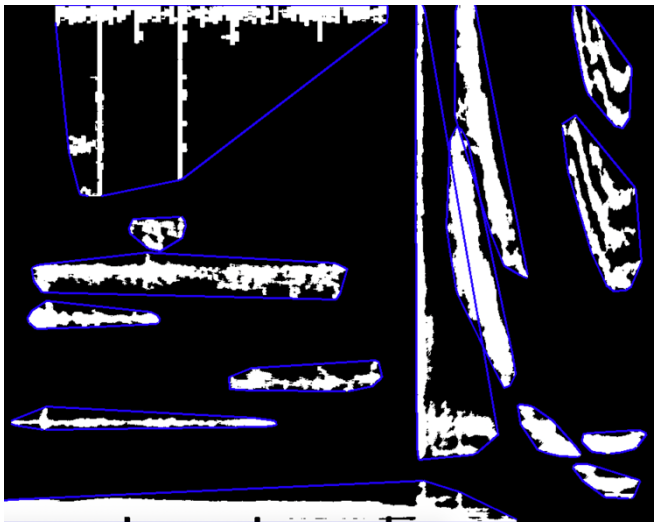

Figure 10: Convex hulls of connected components highlighted on a binarized spectrogram.

The connected components and their respective convex hulls were then used as input to the OpenCV library's *convexityDefects* function, which returns the point on a connected component's edge with maximum distance from the corresponding line in its convex hull [5]. The defects returned from this function for the spectrogram in Figure 10 are shown in Figure 11 as blue points.

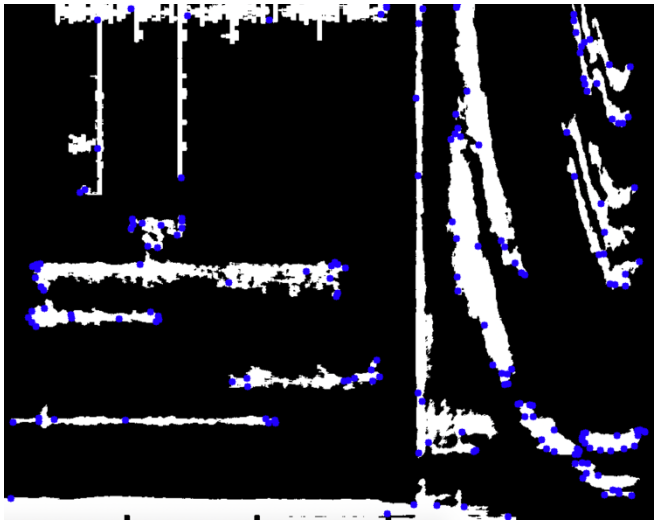

Figure 11: Points furthest away from a corresponding convex hull line highlighted on a binarized spectrogram.

All points in the spectrogram are then filtered out by their defect magnitude (the distance from the corresponding hull line) by

$$\frac{m}{256} > Thresh$$

where $Thresh = 30$ for this project. The magnitude is divided by 256 to obtain the approximate size of the defect in pixels. Displayed in Figure 12 is the spectrogram in Figure 11, but with convexity defects filtered using this method.

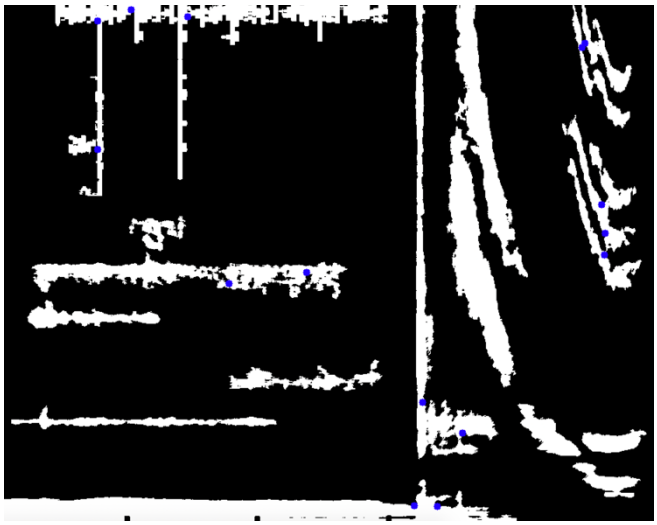

Figure 12: Same points shown on a binarized spectrogram as in Figure 11, but with only those of large defect remaining.

The same points are shown in Figure 13, overlaid on the original grayscale spectrogram in Figure 4.

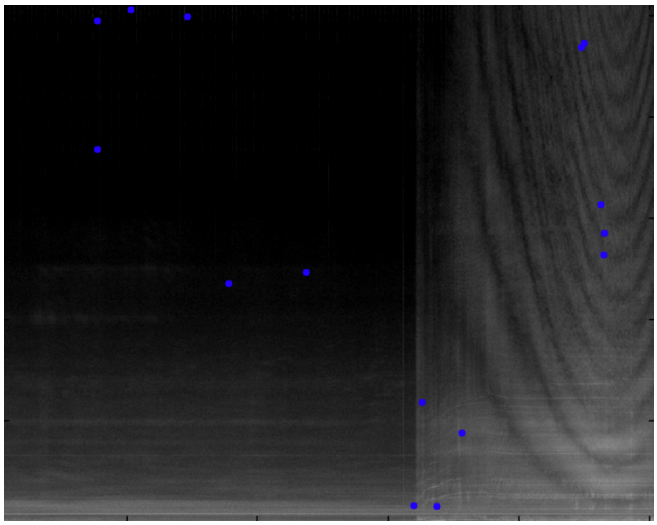

Figure 13: Same points as shown in Figure 12's binarized spectrogram, but overlaid on the original grayscale spectrogram.

Five points are clearly seen to result from the Lloyd's mirror pattern on the right side of Figure 13. The detection of these points and the filtering out of others is the objective of this process.

4) Support Vector Machine Classification

The number of large convexity defects returned by the Lloyd's mirror pattern detection algorithm is combined with the thirteen-bin histogram returned from the tonal detection algorithm to obtain a 14×1 feature vector. This feature vector is supplied to a *LinearSVC* model provided by the open-source Scikit-Learn library, which has been instantiated with a maximum training iteration limit of 100000 using the squared-hinge loss function, L2-regularization, primal optimization, and regularization parameter of 0.8 [5].

The model outputs a 0 if it decides the input spectrogram does not contain a vessel transit and a 1 if it decides that the spectrogram does contain a vessel transit.

IV. Evaluation & Datasets

The dataset of 135 spectrograms used for this project was provided by Tom Dakin of Sea to Shore Systems based in Victoria, British Columbia. It was used to aid the design of the solution detailed in Section III., train the SVM classifier, and evaluate the results. Although the dataset was small, it provided a basis for experimentation and evaluation.

Each of the 135 spectrograms were sourced from the same OceanSonics icListen HF hydrophone located in the Saanich Inlet at approximately 44.65° N and 123.49° W [7]. The spectrograms span a time period of two days, with each containing a five-minute interval of acoustic data. It is noted that the single location and small time period covered by the spectrograms introduces bias towards the time-of-year/month/week and vessel demographic seen. Future experiments are required that use datasets sourced at different locations and times to improve algorithm robustness.

Gillespie's reported results indicate a 90% accuracy of the detector with it recognizing 1897 of 2077 right whale calls labelled by a human operator [2]. Due to the purpose of the detector being to warn ships of possible right whales in an area, the detector had to be tuned away from the parameters that produced the 90% accuracy to reduce the number of false positives – it can be inferred that this was necessary to prevent ships from changing their routes to protect right whales when no right whales were in the area. The detector recognized 60% of calls labelled by a human operator with only 1-2 false positives per day with the new parameters.

Consequences like the diversion of ships are not a necessary consideration in the detection of vessel transits; false positives are more acceptable. False negatives, however, are best avoided – if only spectrograms labelled as containing vessel transits are reviewed by a human, then those labelled as not containing vessel transits will never be caught and corrected. Recall is valued over precision because of this.

The algorithm was tested using 3-fold cross-validation and evaluation of accuracy, precision, recall, and F1-score metrics (more folds would be justifiable with a larger dataset). For each fold, a classifier was trained on feature vectors from a portion of spectrograms processed by the algorithm, then tested on the remaining portion. The classifier outputs during testing were compared against a ground truth set where spectrograms had been manually classified by a human. The results of the 3-fold cross-validation are shown in Table 1.

Fold	Accuracy	Precision	Recall	F1-score
1	0.867	0.870	0.863	0.865
2	0.822	0.857	0.840	0.821
3	0.886	0.875	0.884	0.879

Table 1: Showing the resulting metrics of 3-fold cross-validation.

The results gathered are positive and provide confidence in the algorithm's performance. Due to there being significant differences in the algorithms and evaluation mechanisms used between this project and Gillespie's, comparing the results of one against the other is not insightful. Recall was not always higher than precision, but it did achieve desired scores overall.

Results of the algorithm through manual analysis were also impressive; after reviewing the tonal patterns detected or not detected in spectrograms with vessel transits and without vessel transits, it appeared that the algorithm was highlighting the same tones that a human might choose. When reviewing the number of convexity defects in spectrograms with Lloyd's mirror pattern and without Lloyd's mirror pattern, there appeared to be the desired effect of increased labelled defects with the pattern present.

V. Conclusion

The largely unsolved problem of automatically detecting marine vessel transits in spectrograms means human technicians are required to devote significant time to manual classification. This project addresses that issue by attempting to reduce the number of spectrograms that require manual review by humans. It does so through a process of removing noise, identifying key tones, and identifying the presence of Lloyd's mirror pattern in spectrograms, then classifying the spectrograms via support vector machine. Results were positive and showed significant progress in the problem domain – 3-fold cross-validation showed precisions of 85.7% to 87.5% and, more importantly, recalls of 84% to 88.4%. Future work on this project could include tuning the classifier to work on a more diverse dataset, improving tonal pattern detection, and improving the filtering of convexity defects unrelated to Lloyd's mirror pattern.

VI. References

[1] "Hydrophone Network," *SIMRES*. [Online]. Available: https://www.saturnamarineresearch.ca/hydrophones. [Accessed: 30-Apr-2020].

[2] Douglas Gillespie, "Detection and Classification of Right What Calls Using an 'Edge' Detector Operating on a Smoothed Spectrogram," *Journal of the Canadian Acoustical Association*, Vol. 32 No. 2, 2004.

[3] A. Rezvanifar, T. P. Marques, M. Cote, A. B. Albu, A. Slonimer, T. Tolhurst, K. Ersahin, T. Mudge, and S. Gauthier, "A Deep Learning-based Framework for the Detection of Schools of Herring in Echograms," *arXiv:1910.08215*, 2019.

[4] Derek Bradley and Gerard Roth, "Adaptive Thresholding Using the Integral Image," *Journal of Graphics Tools,* 12(2):13-21, 2007.

[5] "Structural Analysis and Shape Descriptors," *OpenCV*. [Online]. Available: https://docs.opencv.org/3.4/d3/dc0/group__imgproc__shape.html#gac7099124c0390051c6970a987e7dc5c5. [Accessed: 30-Apr-2020].

[6] N. Dalal and B. Triggs, “Histograms of oriented gradients for human detection,” *2005 IEEE Computer Society Conference on Computer Vision and Pattern Recognition (CVPR'05)*, San Diego, CA, USA, 2005, pp. 886-893 vol. 1.

[7] “icListen HF,” *Ocean Sonics*. [Online]. Available: https://oceansonics.com/products/iclisten-hf/. [Accessed: 31-April-2020].